

# Mapping and early-warning of insect defoliation in Scots pine with multi-temporal MODIS data

Thomas, Johansson; Eklundh, Lars

2009

*Lund Electronic Reports in Physical Geography*
**No. 6, June 2009**
**Department of Physical Geography and Ecosystems Analysis**
**Lund University, Sweden**
**ISSN: 1402 – 9006**
**ISBN: 978-91-85793-11-2**

**Reference: *Lund eRep. Phys. Geogr., No. 6, June 2009*.**
**URL: http://www.nateko.lu.se/Elibrary/LeRPG/6/LERPG6Article.pdf**

# Mapping and early-warning of insect defoliation in Scots pine with multi-temporal MODIS data - report to the REMFOR project

Tomas Johansson
Lars Eklundh

## Table of contents



Contact person: Lars Eklundh
e-mail: lars.eklundh@nateko.lu.se

## Abstract

Methods were developed for post-detection and early-warning of defoliation in Scots pine [*Pinus silvestris*] forests in south-eastern Norway caused by the pine sawfly [*Neodiprion sertifer*] with the use of multi-temporal MODIS NDVI 16-day composite data. The post-detection method utilizes summer mean values and seasonal angle (showing whether values have increased or decreased during the season) to identify changed pixels. Damage detection was done by comparing 2005 summer mean and seasonal angle to normal values based on the years 2000 to 2002. In addition to 16-day NDVI the new index Wide Dynamic Range Vegetation Index (WDRVI) was tested. Classification results were evaluated with laser scanned LAI data. The damage classifications with 16-day NDVI had *kappa* coefficients between 0.48 and 0.63, and detected 71% to 82% of the damaged pixels. Although damage classification with WDRVI gave similar results, NDVI was retained for reasons of comparison with other work, and because the behaviour of WDRVI in forest is not yet well known. The developed early-warning method uses calculated differences in NDVI and a seasonal angle between the damage year and a normal year for every 16-day MODIS scene during the growing season. Calculated differences in NDVI and seasonal angle were tested with the Wilcoxon signed rank test for significant changes, and combined into seasonal damage maps. The seasonal damage maps display a consistent pattern through time, indicating the core damage areas with a fair accuracy, when comparing with evaluation data generated by laser scanning. In conclusion, time series of MODIS NDVI can be used for detecting defoliation due to pine sawfly in Norwegian forests, and for early-warning. The damage areas can be coarsely located with fair accuracy. Control of detected damage areas using high resolution remote sensing data or fieldwork is recommended for accurate delineation of the damages.

# 1. Introduction

In 2004, and especially 2005, Scots pine [*Pinus silvestris*] forests in Åsnes, south-eastern Norway were subject to severe outbreaks of the pine sawfly [*Neodiprion sertifer*] (Solberg *et al*., 2006). The larvae of the pine sawfly attack the pine trees in June and start to feed mainly on the last year needles. Thereafter they move on to older needles, and under severe attacks continue with current needles, eventually causing complete defoliation. The trees rarely die, but some severely affected trees may be killed by attacks of the bark beetle [*Tomicus piniperda*] (Skogsstyrelsen, 2007). Outbreaks are usually recurrent for several years causing losses in growth. Satellite derived vegetation indices have the potential to be effective for detecting changes in the vegetation. With multi-temporal data, e.g. from the Moderate Resolution Imaging Spectroradiometer (MODIS) sensor onboard the Terra platform, it is also possible to investigate the intra-annual variations, and therefore these data may be used to map large-scale variations in needle loss caused by the pine sawfly.

This paper serves as a report to the REMFOR project, coordinated by Dr. Svein Solberg, Norsk institutt for skog og landskap, Norway.

## *1.1. NDVI and TIMESAT*

The NDVI is a widely used index for monitoring vegetation and has successfully been used in a number of fields, e.g. classification of land use (Evans *et al*., 1993), estimation of fraction of absorbed photosynthetically active radiation (*f*APAR) (Sellers *et al*., 1994), and net primary production (NPP) (Myneni *et al*., 1997). NDVI is defined as:

$$NDVI = \frac{R_{NIR} - R_R}{R_{NIR} + R_R} \tag{1}$$

where $R_{NIR}$ and $R_R$ are the reflectance values of the near-infrared channel and the visible red channel, respectively.

NDVI data with high temporal resolution, e.g. data from MODIS, makes it possible to study seasonal variations of vegetation. The MODIS NDVI has been used in several studies due to its capability to capture variations in the vegetation, and has shown to be useful in determining the absorption of photosynthetic light in pine and spruce forest canopies (Olofsson, 2007; Olofsson & Eklundh, 2007), estimating net primary production of the boreal forest (Olofsson *et al*., 2007), and for harvest disturbance detection in Northern forests (Jin & Sader, 2005). Even though the MODIS NDVI data has been corrected for atmospheric effects (Vermote *et al*., 2002) there are remaining disturbances affecting the data, e.g. geolocation errors, angular variations, remaining clouds and atmospheric disturbances (Eklundh *et al*., 2007). In order to derive phenological metrics from the data and deal with these effects the software package TIMESAT was developed (Jönsson & Eklundh, 2002, 2004). TIMESAT has been proven useful in many studies of time-series of satellite sensor data, e.g. Eklundh and Olsson (2003), Olsson *et al.* (2005), Seaquist *et al.* (2006), Heumann *et al.* (2007) and Tøttrup *et al.* (2007). TIMESAT fits

smooth model functions to the upper envelope of the NDVI signal for each image pixel and derives a number of phenological parameters.

*1.2. WDRVI*

A common problem in dense vegetation stands is the high degree of light absorption making vegetation indices insensitive to biomass changes. It has recently been shown that the Wide Dynamic Range Vegetation Index (WDRVI) performs better than the NDVI in estimating LAI in high-density crops (Gitelson, 2004; Gitelson *et al*., 2007). While the NDVI becomes saturated with high densities of photosynthetic green biomass and the relationship between NDVI and LAI is non-linear, the WDRVI increases the sensitivity of the NDVI, and hence makes the WDRVI - LAI relationship linear. WDRVI can be calculated from NDVI with the following expression (Viña & Gitelson, 2005):

$$WDRVI = \frac{(\alpha+1)NDVI + (\alpha-1)}{(\alpha-1)NDVI + (\alpha+1)} \quad (2)$$

where $\alpha$ is a weighting coefficient that attenuates the contribution of NIR to the index, leading to an increase in the dynamic range over the NDVI. The value of $\alpha$ depends on sensor characteristics and atmospheric conditions. When $0 < \alpha < 1$ the equation produces the WDRVI and when $\alpha$ is set to 1, the WDRVI is equivalent to the NDVI. It has been noted that a value for $\alpha$ of 0.2 is generally effective for proximal sensing (the use of portable spectral radiometers operating at the same wavelengths as the satellite sensors) of LAI (Gitelson, 2004), for AVHRR data (Viña *et al*., 2004), and for estimation of green LAI in crops with MODIS 250 m data (Gitelson *et al*., 2007), and hence a good starting point when calculating and evaluating the WDRVI. The studies of the WDRVI are mostly done on crops but will be tested here for the Scots pine dominated forest in the study area.

The aim of this study is to create simple methods for post-detection and early-warning of pine sawfly in Scots pine forests of south-eastern Norway. This will be done with MODIS NDVI time-series data, which could be sensitive to large-scale variations in needle loss due to insect damage. For post-detection, the new index WDRVI with possible advantages over the NDVI, will also be tested.

## 2. Materials and methods

*2.1. Data*

In this study multi-temporal NDVI data from the MODIS sensor was used. The MODIS 250 m grid vegetation index product (MOD13Q1) is a 16-day composite (23 scenes/year) that uses daily observations from the MODIS sensor of the Terra satellite. The product is mapped to a sinusoidal projection grid. MOD13Q1 contains two vegetation indices, the NDVI and the Enhanced Vegetation Index (EVI). The MOD13Q1 also includes quality assessment (QA) data (VI Usefulness Index), which assigns a quality flag to each NDVI value. The quality flags are set based on the conditions when the data was recorded (MODIS VI User Guide). A seven-year (2000-2006) time-series data set was used.

In addition to MOD13Q1, 8-day MODIS surface reflectance data was obtained in order to utilize the higher temporal resolution. More data points per time unit (46 scenes/year) potentially makes it possible to get a smoother adjustment of the time-series and a more accurate seasonal profile, and hence better estimations of phenological parameters. The 250 m reflectance grid product (MOD09Q1) is a composite of 8 daily registered observations mapped to a sinusoidal projection grid. Data quality is provided in the enclosed QA science data set. Data for the period 2000-2005 was acquired through the EOS Data Gateway, and NDVI was calculated according to equation 1.

A forest stand map based on 2003 aerial photos was used in order to mask out non-pine forest pixels and clear-cuts. A raster data layer showing percentage pine of the total standing volume (hereafter referred to as *pinepros*), extracted from the forest stand map, was used to mask out pixels having less than 90% Scots pine of the standing volume in order to obtain pure pine forest pixels. In the forest stand map, stands with at least 90% pine classified as clear-cut were extracted and used for masking out clear-cuts because these areas might be detected as insect damage. Both clear-cut and *pinepros* data have a spatial resolution of 10 m and had to be resampled to 250 m for the use with MODIS data.

Change from May to July 2005 in 250 m airborne LIDAR LAI data (hereafter referred to as *LIDAR LAI*) was used in order to establish a relationship with MODIS NDVI, and for evaluation of the damage detection and the early-warning damage maps. *Pinepros*, forest stand map and *LIDAR LAI* data were in the UTM 33N coordinate system and had to be reprojected to MODIS sinusoidal projection for the use with MODIS NDVI data. This was done using a nearest neighbour sampling routine.

*2.2. Pre-analysis*

The re-projected *LIDAR LAI* and pine data were used along with documentation on affected (damaged) areas in order to identify damaged pixels in MODIS. The NDVI time-series and the corresponding quality data of these test pixels were extracted for analysis. Due to the remaining disturbances in MODIS NDVI the data were smoothed with the Savitsky-Golay algorithm of TIMESAT (Jönsson & Eklundh, 2004). The extracted NDVI time-series along with the QA of the selected pixels were used to find the best fit of the

Savitsky-Golay algorithm, and to study the seasonal behaviour of damaged areas. It was observed that both the seasonal amplitude (the summer NDVI level) and the seasonal profile (the shape of the curve during the season) changed during years of insect attacks (Figure 1). For years of no attack the seasonal profile is characterized by a steep increase during the growing season that levels off somewhat in the early summer, but with a second increase during summer creating a positive slope during the middle of the growing season. In insect attack years, the increase in NDVI levels off, resulting in lower amplitude and a flatter or decreasing seasonal profile.

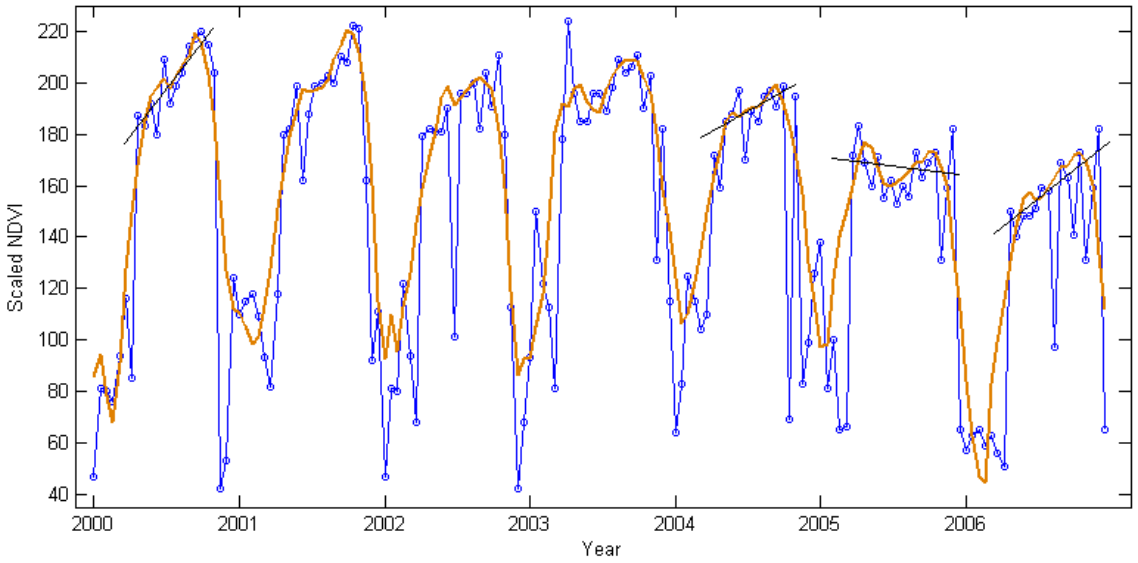


**Figure 1.** Raw and smoothed scaled 16-day $NDVI_{MODIS}$ time-series of a damaged pixel. Note the decrease in amplitude and the changed seasonal angle in 2005, compared to 2000-2002 (illustrated with thin black lines).

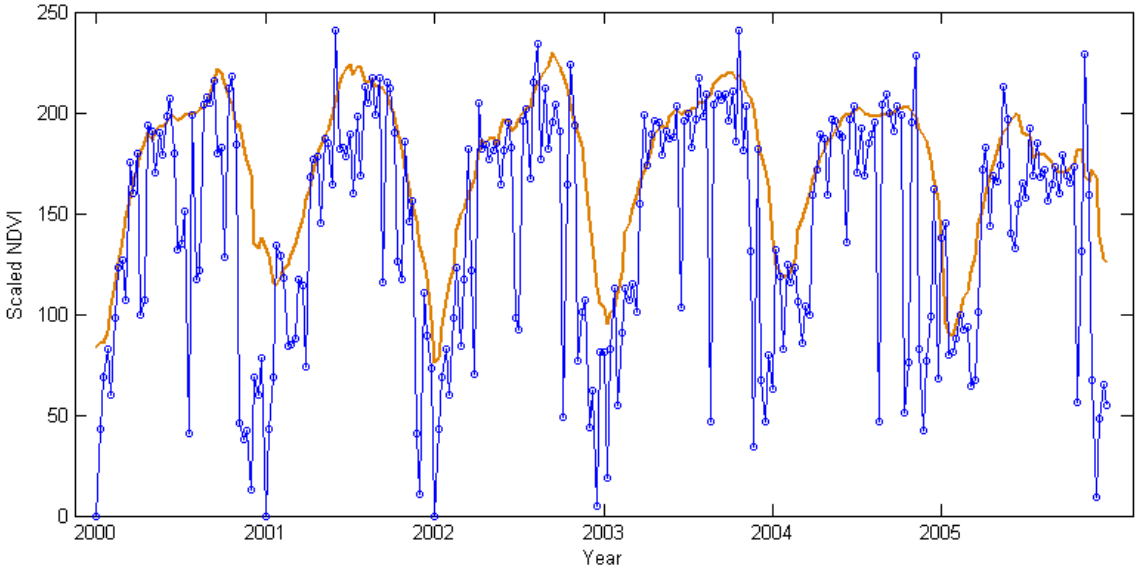


**Figure 2.** Raw and smoothed scaled 8-day $NDVI_{MODIS}$ time-series of a damaged pixel. Noisy data, especially the high values early in the season, affected the adjustment of the seasonal curves.

The 8-day MODIS NDVI calculated from surface reflectance data were also smoothed with the Savitsky-Golay algorithm in TIMESAT (Figure 2). A lot of residual noise in the data, however, made it difficult to find a good fit.

The settings for the Savitsky-Golay algorithm selected with the test pixels was then used for all pixels in a subset of the MODIS scene covering the study area, producing fitted functions and phenology output data such as start and end of season. Both 16-day and 8-day MODIS data were analysed.

In addition to the NDVI the WDRVI was calculated from the smoothed MODIS NDVI time-series according to Equation 2. A range of values of $\alpha$ (0.05, 0.1, 0.2, 0.3, 0.4 and 0.5) was tested in order to assess the performance of the WDRVI over the NDVI. The dynamic range (range from min to max value) of WDRVI was compared to that of NDVI. Figure 3 shows WDRVI together with NDVI for a damaged pixel. The most significant difference that can be noticed in the figure is the slightly different seasonal profile for years with higher VI values (2000, 2001). The summer increase is more extended for the WDRVI, and the difference between the peak values 2000 and 2005, for example, is greater in WDRVI.

**Figure 3.** Smoothed scaled 16-day $NDVI_{MODIS}$ time-series and calculated 16-day $WDRVI_{MODIS}$ of a damaged pixel. While generally lower, the high WDRVI summer values (2000 and 2001) are more emphasized.

*2.3. Summer mean and seasonal angle*

After focusing on the test pixels, the entire study area was processed. For each year a summer mean was calculated based on the phenology output parameters of TIMESAT. The mid point of the season was extracted and a mean value was calculated from the mid point ± one point (± 16 days). Also, a seasonal angle was calculated in order to capture the change in the seasonal profile. The seasonal angle was generated from the slope

during the growing season, showing whether values had increased or decreased during the season. Two methods were applied to obtain the seasonal angle. Method 1 used two endpoints (ep) of the summer period to calculate the angle. The first endpoint in the angle calculation was selected as the mid point – 5 points. The second endpoint was selected by either searching for the highest end of summer point in order to fully capture the typical seasonal behaviour of the pine forest, or if there was a conflict with the first endpoint (second endpoint at the same scene as, or before the first endpoint) the second endpoint was chosen as the mid point + 5 points. NDVI and WDRVI mean values were calculated for each endpoint ($ep_1 \pm 1$ p and $ep_2 \pm 1$ p), and the linear equation was used to calculate the seasonal angle. In method 2 a linear function was fitted to the summer points chosen as the mid point ± 5 points. The angle was calculated from the two end points of the fitted linear function. Figure 4 shows the two methods by which the seasonal angle was generated. Mean values over all pixels for the period 2000-2002 were then generated for both summer means and seasonal angles representing the normal case for pixels with at least 90% pine. These years were chosen because the typical seasonal profile was most evident during the 2000-2002 period, and because some insect attacks had occurred in 2003 and 2004.

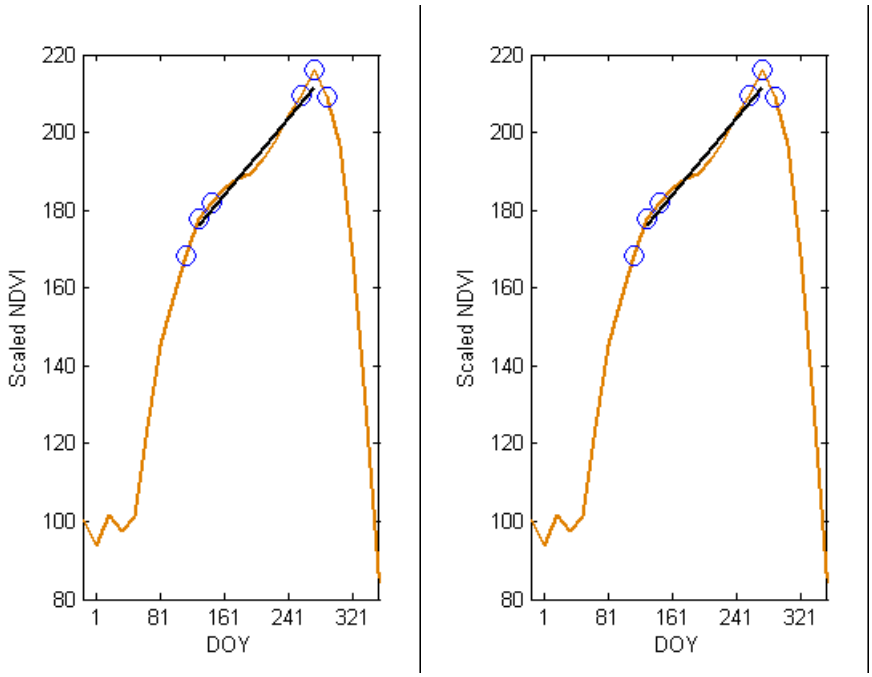


**Figure 4.** The two methods by which extraction of seasonal profile and angle calculation were made. Method 1 (left) selects two end points, calculate a mean for each point ± 1 point, and calculate the seasonal angle. Method 2 (right) fits a line through the summer data points and calculates the angle from the line.

Summer means and seasonal angles were also calculated for the 8-day NDVI. Several deviating values indicating negative trends during normal non-affected years were then observed, instead of the expected positive trend. It was concluded that this originated from noise in the 8-day data. Generally, high erroneous NDVI values in spring or early

summer affected the TIMESAT adjustment for the whole season. Hence, it was decided not to continue the work with 8-day NDVI.

The change from the total mean (2000-2002 normal) to 2005 in summer mean (d_NDVI) and seasonal angle (d_NDVIangle) for all pixels with at least 90% pine were plotted against *LIDAR LAI* (Figure 5). Similar values for WDRVI were also plotted against *LIDAR LAI* (Figure 6) and compared to the corresponding NDVI-LAI change relationships with regression analysis. Due to the generally weak quantitative relationships between these variables it was decided to focus the analysis on qualitative changes between the years (damage classification) rather than attempting to estimate the degree of damage.

*2.4. Damage detection*

A threshold value for damage detection was set as total mean – 1 std. Hence, 2005 pixels with summer mean values AND seasonal angle values below the threshold values were selected as pixels damaged by the pine sawfly. This procedure was applied to both NDVI and WDRVI data sets, and produced damage maps for the study area.

A damage map was also created for a larger area than the study area. Since no mask data on pine (*pinepros*) was available for the larger area an alternative detection algorithm was developed to be used without the masking of non-pine forest pixels. In this case pixels had to be tested for forest (pine) or no-forest. This was done by comparing the normal summer mean and normal seasonal angle for each pixel with lower limit values extracted from the normal case of the 90% pine pixels. The detection of damaged pixels was done in the same way as in the regular damage detection algorithm. Maps were produced for both NDVI and WDRVI. A subset (the study area) of each damage map was extracted for evaluation of the damage classification. All of the produced maps were then reprojected from MODIS sinusoidal to UTM 33N.

*2.5. Evaluation of the damage detection*

The damage maps were evaluated against *LIDAR LAI* in order to estimate the classification accuracy. The pixels classified as damaged were compared to *LIDAR LAI* pixels having negative values (negative trend during the season). Percent correct classified pixels of the total number of pixels with negative values in *LIDAR LAI* (producer's accuracy) and percent correctly classified pixels of the total number of pixels classified as damaged (user's accuracy) were calculated. The damage detection accuracy was also evaluated with the statistical parameter *kappa* (Lillesand et al. 2008).

*2.6. Early-warning method*

The early-warning algorithm was based on calculating the differences in NDVI and seasonal angle between the insect damage year and normal year for each pixel (Figure 1). This was done for every MODIS scene following a starting date. In order to find significant changes, the Wilcoxon signed rank test was used to test the calculated

differences (5% significance level). When a significant negative change was found, the pixel was classified as potentially damaged.

A one-year normal curve was created for every pixel by computing three-year averages of the period from 2000 to 2002 for each MODIS 16-day time step (Figure 5). This three-year period was chosen as the basis for the normal curve because of the lack of reports of insect damages during these years, and the appearance of typical seasonal profiles representing healthy pine trees during these years. In 2003 and 2004 there were minor insect attacks affecting the curve, hence, these years were excluded from the averages.

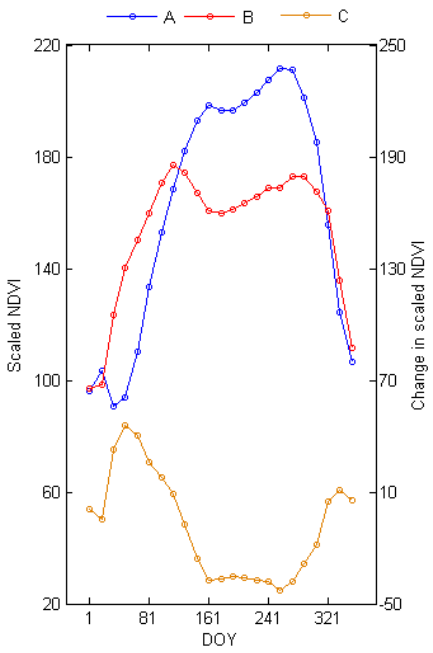


**Figure 5.** Curves for normal year (A), the damage year 2005 (B) and difference between 2005 and the normal year (C) for a damaged pixel.

The sixth MODIS scene (DOY 81, March 22), in early spring, was selected as the starting date. The winter values are, due to snow and clouds, of poor reliability and were not used. Beginning at the starting date the differences in NDVI between the damage year (2005) and the normal year was calculated. Testing with the Wilcoxon signed rank test was started when the first negative difference between the damage year and the normal year had been found. This was done to ensure that only pixels with potential damage were identified. Testing from the first scene with negative difference also allows for earlier detection of potential damaged pixels, as opposed to testing directly from the starting date, which would lead to detection of the first potential damaged pixels much later in the year if any at all.

By fitting a linear function to the data values between the fifth scene and the last added scene, beginning with the starting date, and calculating the slope between the two end points of the fitted function generated the seasonal angle. The seasonal angle of the damage year was compared with the corresponding angle of the normal year. The difference between the two (damage year – normal year) was calculated. When two angle

values had been calculated, i.e. the seventh scene had been added; testing of the angle differences with the Wilcoxon signed rank test was commenced.

For a pixel to be marked as damaged in the early-warning map, the differences in both mean seasonal NDVI and seasonal angle had to be significant for two consecutive scenes. This was done to avoid a pixel from being marked as damaged based on only one significant negative change, possibly not reflecting a consistent change caused by an insect attack but rather a temporary deviation or an effect of noisy data. A pixel marked as damaged in the early-warning map could be unmarked if either the differences in NDVI or seasonal angle were tested as non-significant for the two following scenes. These strict criteria were formulated to make sure that the early-warning method was stable and resistant to minor changes. Also, the method prevented a heterogeneous spatial pattern in the output damage maps. The early-warning damage maps were reprojected from MODIS sinusoidal to UTM 33N.

### *2.7. Evaluation of the early-warning maps*

A formal evaluation was made against the damage map for MODIS scene 16 (DOY 241-256) since this coincided with the date of the *LIDAR LAI* change map. The total damage area at the end of the season (scene 21) was also evaluated for comparison with the damage detection method. The *LIDAR LAI* was used as reference data in the evaluation and producer's accuracy, user's accuracy, as well as the statistical parameter *kappa* were calculated.

## 3. Results

*3.1. Relationships*

The correlation between the change in summer mean MODIS NDVI and the change in *LIDAR LAI* was significant but low, $r^2$ = 0.12 (Figure 6a). Change in seasonal angle (method 1) versus change in *LIDAR LAI* was also weakly correlated, although slightly stronger than for summer mean NDVI, $r^2$ = 0.13 (Figure 6b). Change in seasonal angle (method 2) showed nearly no relationship with change in *LIDAR LAI* ($r^2$ = 0.06).

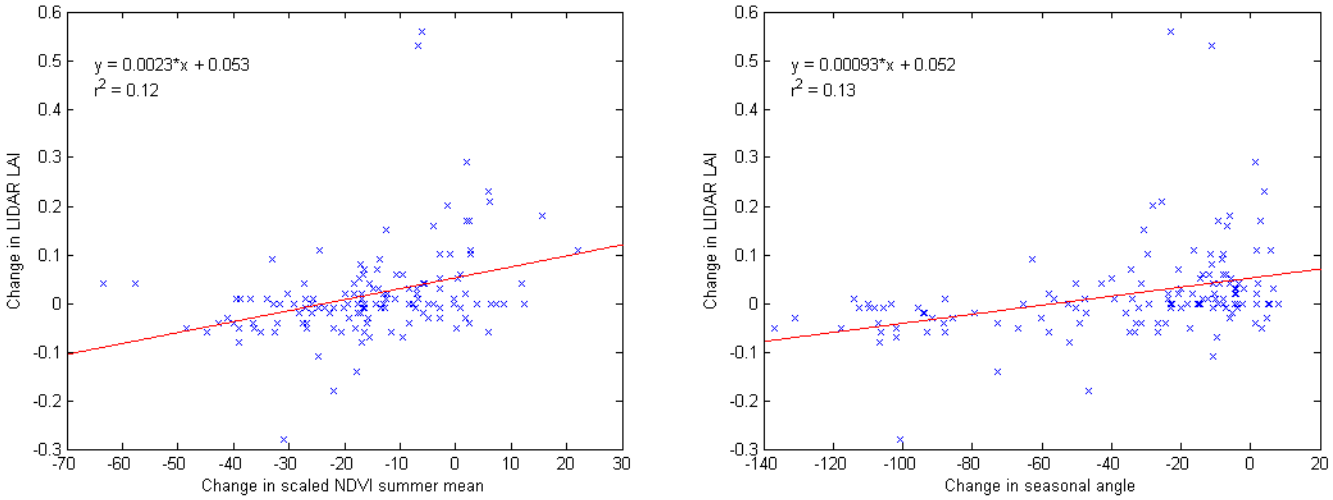


**Figure 6.** Change in $LAI_{LIDAR}$ (May-July 2005) plotted versus change in scaled $NDVI_{MODIS}$ summer mean (a, summer mean 2005 - normal summer mean (2000-2002)) and change in $NDVI_{MODIS}$ seasonal angle, method 1, b, seasonal angle 2005 - normal seasonal angle (2000-2002) for pixels with at least 90% pine.

The dynamic range calculated for the WDRVI showed an increase over the NDVI for all values of α except for 0.05, which instead had a smaller range than NDVI, especially for the seasonal angle. The WDRVI for α = 0.2 had the largest range in both summer mean and seasonal angle. Table 1 shows percentage increase in WDRVI for different values of α over NDVI.

**Table 1.** Change in dynamic range of the WDRVI over the NDVI (α = 1) for summer mean and seasonal angle

| α | Change in dynamic range (%) | |
|---|---|---|
| | Summer mean | Seas. angle |
| 1 | - | - |
| 0.05 | -5.80 | -4.64 |
| 0.1 | 20.62 | 1.97 |
| 0.2 | 32.69 | 4.61 |
| 0.3 | 31.24 | 4.60 |
| 0.4 | 27.05 | 4.28 |
| 0.5 | 22.51 | 3.78 |

When using WDRVI the correlations were slightly better than for the NDVI. Scatterplots of the relationship between d_WDRVI-*LIDAR LAI* ($r^2$ = 0.13) and d_WDRVIangle-*LIDAR LAI* ($r^2$ = 0.14) for α = 0.2 can be seen in Figure 7. The relationship between change in seasonal angle (method 2) and change in *LIDAR LAI* was also very weak with WDRVI ($r^2$ = 0.07).

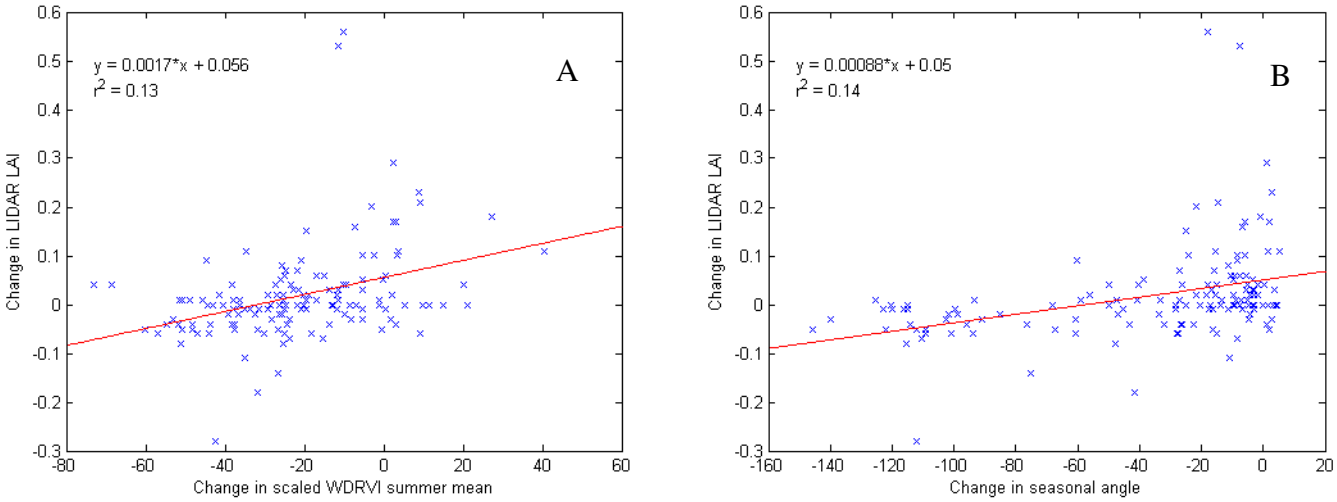


**Figure 7.** Change in $LAI_{LIDAR}$ (May-July 2005) plotted versus change in scaled calculated $WDRVI_{MODIS}$ summer mean (A, summer mean 2005 - normal summer mean (2000-2002)) and change in $WDRVI_{MODIS}$ seasonal angle, method 1, (B, seasonal angle 2005 - normal seasonal angle (2000-2002)) for pixels with at least 90% pine (α = 0.2 was used).

Table 2 shows summary statistics for the regression analysis. It can be seen that all of the regressions are significant, but that the correlation coefficients do not differ considerably from each other. Of the weak relationships WDRVI at α = 0.1 and 0.2 have the strongest correlation. The regression analysis also shows that both summer mean and seasonal angle make significant contributions to the total correlation. Based on the calculated WDRVI with the largest dynamic range and the best correlation, an α value of 0.2 was chosen when working with the WDRVI in the damage detection algorithm. The difference between the NDVI-LAI and WDRVI-LAI total correlations were not significant ($p$ = 0.47).

**Table 2.** Regression analysis statistics for NDVI (α = 1) and WDRVI for different values of α versus *LIDAR LAI*. In the model regression is tested with both summer mean and seasonal angle. 5% significance level.

| α | $r^2$ | F | P |
|---|---|---|---|
| 1 | 0.167 | 13.870 | 0.000 |
| 0.05 | 0.170 | 14.180 | 0.000 |
| 0.1 | 0.173 | 14.481 | 0.000 |
| 0.2 | 0.173 | 14.465 | 0.000 |
| 0.3 | 0.172 | 14.368 | 0.000 |
| 0.4 | 0.171 | 14.274 | 0.000 |
| 0.5 | 0.171 | 14.192 | 0.000 |

*3.2. Damage detection*

The produced damage maps based on NDVI and WDRVI are shown in Figure 8 together with standwise predicted LAI loss based on LIDAR. The increased sensitivity in the dynamic range in WDRVI over the NDVI is not reflected in the damage maps (method A). In comparison with the *LIDAR LAI* defoliation map the damage maps cover the main damage areas fairly well, but with some areas overestimated. There are stands that were clear-cut during winter 2004-2005 that show no change in the *LIDAR LAI* defoliation map but appears as damaged in the NDVI and WDRVI maps due to the fact that this is change from normal (2000-2002) to 2005. Although some discrepancies occur, in general the algorithm finds the damaged areas and produces a map with adequate consistency with the *LIDAR LAI* defoliation map. Figure 8 (method D) shows the damage map for NDVI produced with angle calculation method 2 and with the 2003 clear-cuts removed. It can be seen that the classification becomes more conservative than with the angle calculation of method 1. It is also apparent that a larger part of the unchanged areas in the *LIDAR LAI* defoliation map are not classified as damaged, as they are with method A. The damage map generated without the pine forest mask (method E) detects the major damage patterns but clearly overestimates the damage area.

*3.3. Evaluation of the damage detection*

The linear relationships between d_NDVI – *LIDAR LAI* and d_NDVIangle – *LIDAR LAI* were weak, however the damage maps are generally in agreement with the *LIDAR LAI* defoliation map. A count of damaged pixels selected by the algorithm and *LIDAR LAI* pixels with negative values was done to estimate the classification accuracy of the maps. The result of the evaluation can be seen in Table 3 with producer's accuracy, user's accuracy, and *kappa*. With angle method 1, 55 pixels in *LIDAR LAI* were negative (damaged) and 88 pixels were selected as damaged by the damage detection algorithm. 45 of these pixels were the same as in *LIDAR LAI*, hence 51% of the selected pixels were correctly classified as damaged (user's accuracy) and the algorithm detected 82% of the damaged *LIDAR LAI* pixels (producer's accuracy). *Kappa* for this method was 0.48. The major part of the selected pixels that did not show up in *LIDAR LAI* was located in the areas that had been clear-cut.

**Table 3.** Accuracy assessment of the damage detection with MODIS NDVI and WDRVI.

| Method | Producer's accuracy (%) | | User's accuracy (%) | | Kappa | |
|---|---|---|---|---|---|---|
| | NDVI | WDRVI | NDVI | WDRVI | NDVI | WDRVI |
| A | 82 | 82 | 51 | 51 | 0.48 | 0.47 |
| B | 82 | 82 | 53 | 52 | 0.50 | 0.49 |
| C | 71 | 65 | 65 | 65 | 0.63 | 0.63 |
| D | 71 | 65 | 64 | 64 | 0.62 | 0.62 |
| E | 76 | - | 23 | - | 0.12 | - |
| F | 27 | - | 28 | - | 0.19 | - |

Method refers to way the damage maps were produced with different angle calculations, whether 2003 clear-cut areas were removed and if masking of non-pine forest areas was applied. A = angle method 1, B = angle method 1, clear-cuts removed, C = angle method 2, D = angle method 2, clear-cuts removed, E = no pine mask, angle method 1 F = same as E but angle method 2.

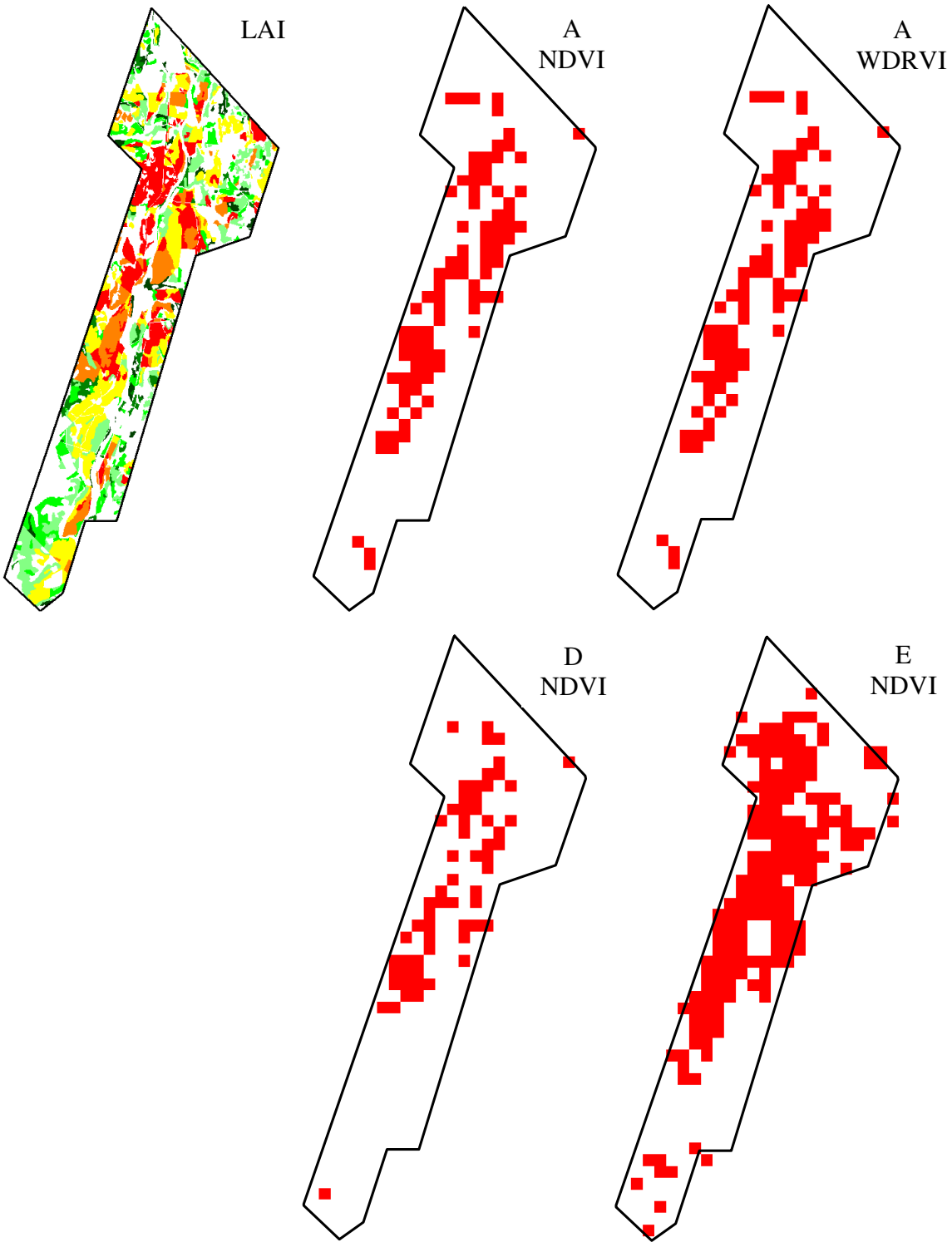


**Figure 8.** Standwise predicted LAI loss based on airborne LIDAR (top left), on a scale from green (clearly increasing LAI = no defoliation) to red (clearly decreasing LAI = severe defoliation). Capital letters refers to damage detection method, where A show damage maps by NDVI and WDRVI ($\alpha$ = 0.2) with angle calculation of method 1. D is NDVI with angle calculation method 2 and with removal of 2003 clear-cuts, and E is NDVI without the pine forest mask. Areas shown have at least 90% of the standing volume as Scots pine (except E).

In the forest stand map based on aerial photos from 2003 some stands with at least 90% pine are classified as clear-cuts. Since these stands may have been harvested in 2003 or earlier, and because the damage detection algorithm makes a comparison between normal values based on 2000-2002 and 2005 these areas will show up as insect damage. A removal of these areas prior to the comparison resulted in 53% of the selected pixels being correctly classified and *kappa* increasing to 0.50.

With angle method 2, the relationship between d_NDVIangle and *LIDAR LAI* was very weak ($r^2$ = 0.06) but the damage map produced when using this method has the greatest *kappa* accuracy, 0.63 and 0.62 with the removal of 2003 clear-cuts (C and D in Table 3). The damage maps produced using angle calculation method 1 (A and B) have lower kappa values than the maps produced using angle calculation method 2 (C and D). However, producer's accuracy is higher for A and B, which means that the detection algorithm finds more of the damaged *LIDAR LAI* pixels than in C and D. The maps of C and D have a lower total number of selected pixels and thus a higher user's accuracy and *kappa*.

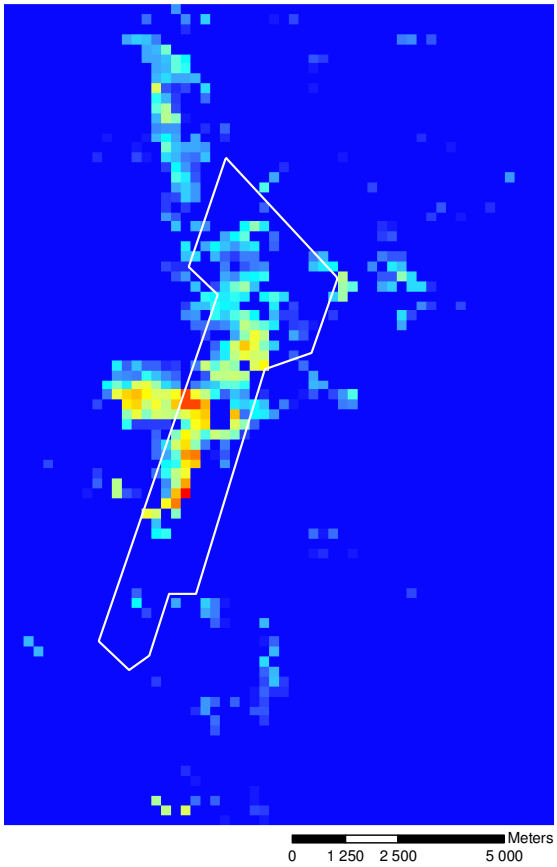


**Figure 9.** Negatively changed areas (normal-2005) for $NDVI_{MODIS}$ (left) represented by change in summer mean NDVI, where blue is no change and red is large decrease.

Evaluation of WDRVI without the pine forest mask is not presented due to the low accuracy of NDVI with the same method, and because of the small difference between NDVI and WDRVI.

In the algorithm without the pine mask, pixels were selected for an area larger than, but covering the study site. The result of the classification is shown in Figure 9 as a change map, providing an overview of where the greatest decrease had occurred. The change shown is from the normal threshold value for the summer mean to the 2005 summer mean ranging from blue (no change) to red (large change).

*3.4. Early-warning*

The first significant changes were detected for MODIS scene 14 in late July – beginning of August (DOY 209-224), and the number of detected pixels increases during the year up to scene 21 (DOY 321-336) that have the highest number of detected pixels. After scene 21 the tests of the differences between test year and normal case for the detected pixels are becoming non-significant due to smaller differences (Figure 5). The seasonal development can be seen in Figure 10. The appearing spatial pattern seems to visually agree with the *LIDAR LAI* defoliation map.

For the damage map of scene 16, 47% of the damaged pixels in *LIDAR LAI* were detected (producer's accuracy) and 53% of the selected pixels were correctly classified as damaged (user's accuracy). *Kappa* for this map was 0.50. Producer's accuracy for the total damage area was 78%, user's accuracy 52%, and *kappa* was 0.49. These results are in good agreement with the evaluations of damage maps produced with the post-damage detection method.

Some of the pixels marked as damaged were located outside the major clusters creating somewhat speckled maps. In an attempt to avoid this, a filtering technique was employed. Every marked pixel was checked for solitary status in a 3x3 window. If the target centre pixel had no marked neighbour pixel in the window, then the target pixel was unmarked. When filtering was applied, the user's accuracy in the evaluation of scene 16 was higher (59%) but the producer's accuracy was lower (42%). The *kappa* value increased to 0.56. For scene 21 producer's accuracy was 76%, user's accuracy 55%, and *kappa* was 0.52. The resulting early detection damage maps are not presented here.

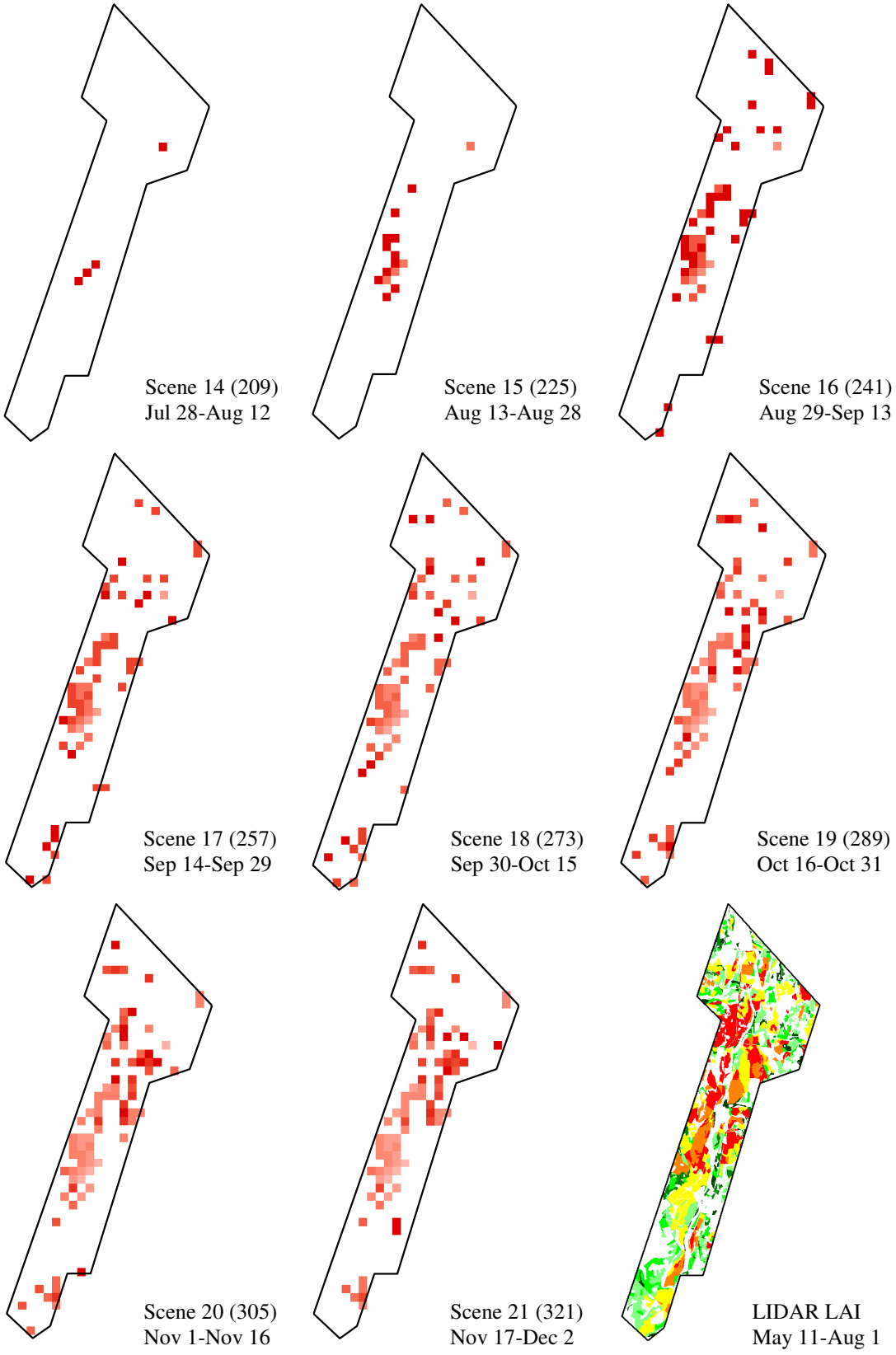


**Figure 10.** Damage maps for corresponding MODIS scenes, DOY of the starting date in brackets. Dark red indicates newly detected pixels for that scene and light red showing pixels detected earlier. The bottom map shows standwise predicted LAI loss based on helicopter LIDAR, on a scale from green (clearly increasing LAI = no defoliation) to red (clearly decreasing LAI = severe defoliation).

## 4. Discussion and conclusions

*4.1. Damage detection*

Although the linear correlations of d_NDVI – *LIDAR LAI* and d_NDVIangle – *LIDAR LAI* were weak, the damage maps produced are generally in good agreement with the *LIDAR LAI* defoliation map, and the main damage areas are identified. The majority (about 65%) of the selected damage pixels coincided with the *LIDAR LAI* pixels for the best classifications.

An overestimation of the damage areas occurs because the algorithm identifies also some winter clear-cut areas and classifies them as damaged. If the change in LIDAR LAI had been calculated from 2004-2005 the agreement might have been stronger, but then falsely accepting clear-cut areas as insect attacks. Removal of the 2003 clear-cut areas resulted in a higher percentage correctly classified damage pixels of the total selected compared to no removal. This indicates that exclusion of the 2004-05 clear-cuts may have increased the percent correctly classified pixels of the total number of pixels classified as damaged even more.

When mapping defoliation, it is difficult to eliminate clear-cut areas because these areas show a greater change in both summer mean and seasonal angle than areas damaged by insect attack, especially when comparing to a "normal" value as in this case. With an insect attack needles are lost, but depending on the magnitude of the attack the trees will not loose all the needles. The remaining needles, as well as the stems and branches will contribute to the NDVI. In contrast, harvesting removes the whole trees and lowers the NDVI, especially on the site of the study area where little, or no green vegetation is present in the ground layer. In an operational detection analysis, separating clear-cuts from insect damage using additional data may be required to handle this problem.

The fact that some minor damage areas are not visible in the damage maps may be owed to the resampling of the pine data. Small areas in 10 x 10 m with 90% pine or more can, when resampled to 250 x 250 m, get a lower percentage value and will therefore be excluded in the masking.

Given the greater dynamic range in the new index WDRVI over the NDVI the WDRVI may be a better choice if an estimation of the magnitude of change is wanted. The WDRVI is more sensitive in denser vegetation than the NDVI, and might be more suitable for weak defoliation events in denser, spruce forests. However, given the insignificant improvement in the present study NDVI is retained since it is a standard product in many databases, for easier comparison with other work, and because the behaviour of WDRVI in forest is not yet well known. The use of 8-day NDVI did not generate acceptable results, and was abandoned.

Method 2 of angle calculation gives a more conservative result in the damage detection than angle calculation method 1. Hence, if cautious damage estimation is wanted, detection with angle method 2 is preferred. On the other hand, when using method 1 in the damage detection 82% of the damaged pixels in *LIDAR LAI* are found. To be sure to

find as many damaged pixels as possible detection with angle calculation method 1 should be used, and if possible with data of clear-cuts included for best result.

*4.2. Early-warning*

The results show that multi temporal MODIS NDVI can be used in a detection method for early-warning of pine sawfly attacks. The first signs of damage attacks are spotted with MODIS scene 14, or DOY 209, in July. In general, the larvae of the pine sawfly start feeding on the needles in June and hence, the first pixels detected by the method appears ca a month later. By scene 16, DOY 241, in late August, the spatial patterns are more evident with some clusters of pixels. Considering that this method was developed with 16-day temporal resolution, a delay of two months from the initial feeding of the needles to detection of the major damage areas is satisfactory. It is possible that data with a higher temporal resolution, i.e. 8-day MODIS NDVI, could lead to earlier detection of the damage areas, although this was not tested here.

A spatial filtering technique was applied to eliminate solitary pixels from the damage maps. This was done primarily to avoid the speckled appearance of the maps and to maintain only the larger damage areas. Although the maps became more homogeneous, some correctly classified pixels over smaller damage areas were removed and thus, decreased the producer's accuracy. However, the user's accuracy increased as well as the statistical parameter *kappa*, suggesting that filtering could be a useful approach to identifying the major damage areas, although excluding some smaller damage areas.

A criterion that the calculated difference in either NDVI or seasonal angle had to be tested as non-significant for two consecutive scenes was employed to avoid marking and unmarking of pixels from scene to scene. Despite this, a few pixels still showed this behaviour. These pixels are mostly solitary and located outside the major damage areas, and would be eliminated if filtering were applied. This is another indication that filtering may be an appropriate technique.

It should be noted that the methods presented in this paper were developed for the sparsely stocked Scots pine forests of the investigation area, growing on sites with little or no green ground vegetation. Reflected radiation from both the ground and the tree canopy interact and hence, the seasonal NDVI curve is specific for different areas. Depending on the tree species and the ground vegetation the NDVI curve will change, why these specific methods may have to be modified to be applicable to forests in other areas.

In conclusion, 16-day MODIS NDVI time series data can be used for detecting defoliation and early-warning of pine sawfly attacks in the pine forests typical of south-eastern Norway. Although the degree of defoliation is difficult to detect, the damage areas can be coarsely located with fair accuracy. Control of these areas using high resolution remote sensing data or fieldwork is recommended for accurate delineation of the damages. The developed early-warning method identified the core damage areas early

in the season, and the total damaged area at the end of the season corresponded well with the *LIDAR LAI* defoliation map.

## References


Eklundh, L. & Olsson, L., (2003), Vegetation index trends for the African Sahel 1982-1999. *Geophysical Research Letters*, 30:1430-1433.

Eklundh, L., Jönsson, P. and Kuusk, A., (2007), Investigating modelled and observed Terra/MODIS 500-m reflectance data for viewing and illumination effects. *Advances in Space Research,* 39:119-124.

Evans, D.L., Zhu, Z. & Winterberger, K., (1993), Mapping forest distributions with AVHRR data. *World Resource Review*, 5:66-71.

Gitelson, A.A., (2004), Wide Dynamic Range Vegetation Index for remote quantification of biophysical characteristics of vegetation. *Journal of Plant Physiology*, 161:165-173.

Gitelson, A.A., Wardlow, B.D., Keydan, G.P., *et al*., (2007), An evaluation of MODIS 250-m data for green LAI estimation in crops. *Geophysical Research Letters*, 34, L20403, doi:10.1029/2007GL031620.

Heumann, B.W., Seaquist, J.W., Eklundh, L., *et al*., (2007), AVHRR Derived Phenological Change in the Sahel and Soudan, Africa 1982 – 2005. *Remote Sensing of Environment*, In press, available online.

Jin, S. & Sader, S.A., (2005), MODIS time-series imagery for forest disturbance detection and quantification of patch size effects. *Remote Sensing of Environment*, 99:462-470.

Jönsson, P. & Eklundh, L., (2004), TIMESAT – a program for analysing time-series of satellite sensor data. *Computers and Geosciences*, 30:833-845.

Lillesand, T. M., Kiefer, R. W., Chipman, J. W., 2008, *Remote sensing and image interpretation, sixth edition*. John Wiley, 756 pp.

Myneni, R.B., Keeling, C.D., Tucker, C.J., *et al*., (1997), Increased plant growth in the northern high latitudes from 1981 to 1991. *Nature*, 386:698-702.

Olofsson, P., (2007), Remote Sensing of Carbon Balance across Scandinavian Forests. *Meddelanden från Lunds universitets geografiska institution*, Avhandlingar, nr. 169, PhD thesis, Lund: Lund University.

Olofsson, P. & Eklundh, L., (2007), Estimation of absorbed PAR across Scandinavia from satellite measurements. Part II: modeling and evaluating the fractional absorption. *Remote Sensing of Environment,* 110:240-251.

Olofsson, P., Eklundh, L., Lagergren, F., *et al*., (2007), Estimating Net Primary Production for Scandinavian forests using data from Terra/MODIS. *Advances in Space Research,* 39:125-130.

Olsson, L., Eklundh, L. & Ardö, J., (2005), A recent greening of the Sahel—trends, patterns and potential causes. *Journal of Arid Environments*, 63:556-566.

Seaquist, J.W., Olsson, L., Ardö, J. *et al*., (2006), Broad-scale increase in NPP Quantified for the African Sahel, 1982-1999. *International Journal of Remote Sensing*, 27:5115-5122.

Sellers, P.J., Los, S.O., Tucker, C.J., *et al*., (1994), A global 1° by 1° NDVI data set for climatic studies. Part 2: The adjustment of the NDVI and generation of global fields of terrestrial biophysical parameters. *International Journal of Remote Sensing*, 15:3519-3546.

Solberg, S., Næsset, E., Holt Hanssen, K., *et al.*, (2006), Mapping defoliation during a severe insect attack on Scots pine using airborne laser scanning. *Remote Sensing of Environment*, 102:364-376.

Tøttrup, C., Schultz Rasmussen, M., Eklundh, L., *et al*., (2007), Using 250-meter spatial resolution MODIS data and regression tree modeling to map fractional land cover across the highlands of mainland Southeast Asia. *International Journal of Remote Sensing*, 28:23-46.

Vermote, E.F., El Salaeous, N.Z. & Justice, C.O., (2002), Atmospheric correction of the MODIS data in the visible to middle infrared: first results. *Remote Sensing of Environment*, 83:97-111.

Viña, A., Gitelson, A.A., (2005), New developments in the remote estimation of the fraction of absorbed photosynthetically active radiation in crops. *Geophysical Research Letters*, 32, L17403, doi:10.1029/2005GL023647.

Viña, A., Henebry, G.M. & Gitelson, A.A., (2004), Satellite monitoring of vegetation dynamics: Sensitivity enhancement by the wide dynamic range vegetation index. *Geophysical Research Letters*, 31, L04503, doi:10.1029/2003GL019034.


## Internet sources


MODIS VI User Guide.
http://tbrs.arizona.edu/project/MODIS/UserGuide_doc.php, 2007-11-15.

Skogsstyrelsen, (2007), Angrepp av röd tallstekel runt Lima och Malung.
http://www.svo.se/episerver4/templates/SNormalPage.aspx?id=35059, 2007-11-17.